Fracture Mechanics Studies of a Cracked Pipe Bend Under In–Plane Loading

S. Brosi, R. Wanner
Paul Scherrer Institute, Villigen PSI, Switzerland
D. Uhlmann, H. Diem
MPA, University of Stuttgart, Stuttgart, FRG

INTRODUCTION

In cyclically loaded piping components, cracks may initiate and subsequently grow after a sufficient number of load cycles (Kussmaul et al, 1984). This process was studied with the experiment RORV(B) within Phase II of the German HDR Safety Program. Under the operating conditions: internal pressure $p_i = 10.6$ MPa, temperature $T = 240$ °C and elevated oxygen content in the pressure medium (about 8 ppm), a fullsize bend (DN400) of the piping (Fig. 1) was loaded with an in–plane bending moment acting in opening mode by cyclic deflection of one pipe end. After 2007 load cycles the piping failed due to the macroscopically dominating longitudinal crack which was embedded in the fatigue–induced multiple crack field (Diem et al, 1989; Hunger et al, 1989). Surprisingly, the leak occured in the thicker elbow flank. The maximal wall thickness of the two bend shells ($\varphi = 0° \sim 180°$, $180° \sim 360°$) differed by 5% due to the mandrel process manufacturing. Extensive pre–experimental calculations (Uhlmann, 1989) were performed for the longitudinal crack located at the inner surface for the two selected crack lengths $2\alpha_c = 30°$ and $80°$ using a bend model with constant wall thickness. In the post–experimental calculations (Brosi et al, 1989) summarized in the present report the influence of the wall thickness variation on the maximal elbow strains is studied for the unflawed bend; furthermore, the given fracture mechanics studies are completed by the data for the experimentally determined crack length $2\alpha_c = 60°$.

NUMERICAL ANALYSIS

The structural mechanics study was performed using the finite element program ADINA. Large deformations and material nonlinearities were considered by the "Updated Lagrange" formulation and an elastic–plastic material model. The effective stress–strain data of the RORV(B) pipe material (15NiCuMoNb5) were measured in an uniaxial tensile test. In order to consider the variation of both the wall thickness (Fig. 3) caused by manufacturing and of the bending moment along the pipe axis, a full bend ($\alpha = 0° \sim 90°$, $\varphi = 0° \sim 360°$) was isolated from the piping (Fig. 1) and for the finite element analysis discretized as shown in Fig. 4. The straight pipe ends (Fig. 2) of length three times the inner diameter D_i prevent influences from the models boundary conditions on the elbow stresses. In the sectional plane A–A, all displacements were fixed. The static internal pressure was applied by pressure elements at the inner surface and by p_{ax}, the distributed stress component resultant normal to the sectional plane B–B. In a first load step the action of the internal pressure only was calculated. The monotonically increasing force of the hydraulic cylinder and the resulting reaction of the link are reduced to the forces F_x and F_y and the bending moment M_b, acting in the terminal plane B–B; these were incrementally increased in further load steps. For the crack analysis reduced models (Fig. 11) with two symmetries and a quarter of the original size were considered, where the variations of wall thickness and bending moment were symmetrized. The crack depth was constant along its length; except the crack end where its shape was circular. For cracks of length $2\alpha_c = 60°$ and different crack depths a/t = 0.5, 0.75 and 1, J–values were calculated by the energy release method (DeLorenzi, 1980).

RESULTS

The relation between the load controlled numerical analysis and the travel controlled experiment can be evaluated by comparing calculated and measured elbow strains. Of the measured circumferential and longitudinal strains, only the largest ones during the first cycle were sampled. Figg. 5,6 and 7 show that in the elbow apex these strains agree best with the calculated strains in the range between load steps 7 and 8, which corresponds to an average bending moment $M = 1.15$ MNm acting at the elbow apex center. The agreement turned out to be good along the whole cicumference. From this good agreement it may be concluded that the whole calculated elbow strain state is realistic, and that the straight pipe pieces prevent influences from the simplified boundary conditions of the sectional planes A–A and B–B on the bend. Close to these sectional planes some deviations between the calculated strains of the load steps 7 to 8, which is shown by the shaded area in Fig. 5, and the measured strains were expected, but they are still of acceptable magnitude.

From Figg. 8 and 9 it can be seen that a pipe elbow, loaded by static internal pressure and a quasistatic in–plane bending moment in opening mode, reacts by ovalization of its cross–section, i.e. the initial round cross–section of the apex changes its shape to become a sort of oval with its shortest diameter normal to the elbow plane. Due to this ovalization, maximal tensile strains appear in the elbow flanks at the inner surface in circumferential direction (Figg. 6,7) and will cause longitudinal cracks in the case of cyclic loading. The degree of ovalization (ratio of major to minor radius) as well as the greatest circumferential strains are about 5% higher in the thinner elbow flank (Figg. 6,9), i.e. contrary to what one might have inferred from the experiment, the ovalization does not correspond to a travel controlled elbow loading. From the calculated strains it may be concluded that also the cyclic strain magnitudes would be larger in the thinner elbow flank, and that therefore cracks should initiate earlier and grow faster in this area. Thus other effects, such as material inhomogeneities or surface imperfections, might explain the experimentally determined preference of crack initiation or crack growth in the thicker elbow flank.

In the pre–experimental numerical study (Uhlmann, 1989), different crack edge locations for the maximal J–values were found for two selected part–through cracks of length $2\alpha_c = 30°$ and $80°$. The study showed that for deep surface cracks with increasing bending moment the location of maximum J–values can change from the apex to the crack edge end. In Fig. 10 J–values are plotted for the experimental measured crack length $2\alpha_c = 60°$ versus the apex moment. For the two considered crack depths $a/t = 0.5$ and 0.75 the maximal J–values appear at the bend apex for any load level. With increasing surface crack depth, J increases more at the crack end than at the bend apex, but up to the crack depth $a/t = 0.75$ the maximum remains at the apex. This finding agrees well with the leak before break behaviour of the experiment. The calculated J–values are considerably larger than the crack initiation value J_i (Roos et al, 1988). This result was verified by the fractographic analysis, from which it must be assumed that to the fatigue crack growth was superposed a stable crack growth. For through cracks the greatest J–values are the most interesting ones; they are attained close to the inner pipe surface. These values are considerably larger than the maximum J–values of the part–through cracks (Fig. 10).

Figg. 12 and 13 show that for part–through cracks the flexibility of the pipe increases only slightly with increasing crack depth or with increasing crack length, but it changes significantly between part–through and fully through cracks. Furthermore, from Fig. 13 it can be seen that in the case of through cracks the pipe flexibility is greatly influenced by the crack length.

CONCLUSIONS

For a pipe bend under in–plane bending the influence of wall thickness variation on crack initiation was studied; furthermore, J–values were calculated along the crack edge for longitudinal cracks at the bend flanks, having the experimentally determined crack length $2\alpha_c = 60°$. Only the monotonically increasing part of the first load cycle was considered.

- Good agreement was found for calculated and measured strains.
- The deflections normal to the bend axis plane of the two bend flanks differ inversely to the wall thicknesses; therefore the circumferential strains are sligthly larger in the thinner pipe flank.
- The range of the cyclic strains could only be found by a calculation of a further full load cycle, but due to the theoretical investigations it may be assumed that the strain range is about 5% larger in the thinner bend flank. The observed preference of crack growth in the thicker bend flank might be explained by material inhomogeneities or by surface imperfections.
- From the calculated J–values and the fractographic analysis it must be assumed that to the fatigue crack growth was superposed a stable crack growth.
- The maximum J–values are found at the bend apex for all considered surface cracks.
- For an identical crack length, the J–values are considerably larger for a through crack than for a surface crack.
- The pipe flexibility is only slightly influenced by length and depth of part–through cracks, but it is greatly influenced by the length of through cracks.

ACKNOWLEDGEMENTS

We wish to express our gratitude to Dr. R. Rösel from the Paul Scherrer Institute for his support to the presented work. The project was sponsored by the German Ministry of Research and Technology. We gratefully mention the financial assistance from the Swiss Federal Nuclear Safety Inspectorate and from the Swiss Federal Office of Energy.

REFERENCES

Brosi, S., Wanner, R., Uhlmann, D. and Diem, H. (1989): Nachrechnungen zum Rohrversagensversuch RORV(B). MPA–Prüfungsbericht 815518, in preparation.

Diem, H., Blind, D., Katzenmeier, G. and Hunger, H. (1989): Crack initiation and crack propagation of an elbow under in–plane bending in high temperature water of elevated oxygen content. Transaction of the 10th SMIRT–Conference, Los Angeles.

Hunger, H. and Diem, H. (1989): Pipe failure tests (RORV) at HDR facility – experimental results. Transaction of the 10th SMIRT–Conference, Los Angeles.

Kussmaul, K., Blind, D. and Jansky, J. (1984): Rissbildung in Speisewasserleitungen von Leichtwasserreaktoren. VGB Kraftwerkstechnik, 64 Jahrgang, Heft 12, pp 1115–1129.

DeLorenzi, H. G. (1980): On the energy release rate and the J–integral for 3–D crack configurations. General Electric TIS report 80CRD113.

Roos, E., Eisele, U. (1988): Determination of the material characteristics value in the elastic plastic fracture mechanics by means of J–integral crack resistance curves. Journal of Testing and Evaluation, 1.

Uhlmann, D. (1989): Vorausrechnungen zum Rohrversagensversuch RORV(B), MPA–Prüfungsbericht 815517001 uh/na.

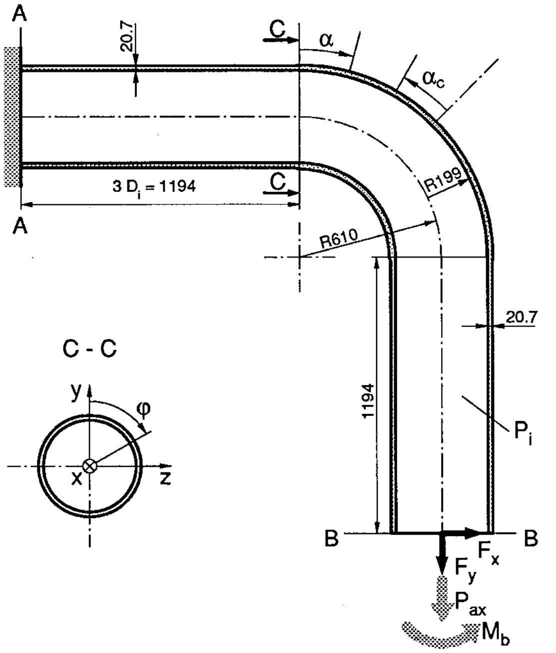

Figure 2 Geometry, boundary conditions and co-ordinate systems of the finite element model.

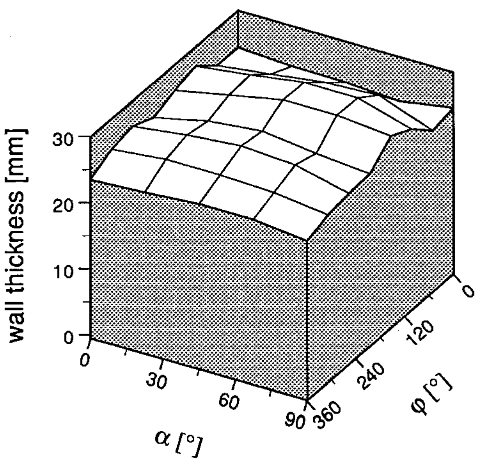

Figure 3 Variation of the elbow wall thickness (elbow manufactued by the mandrel process).

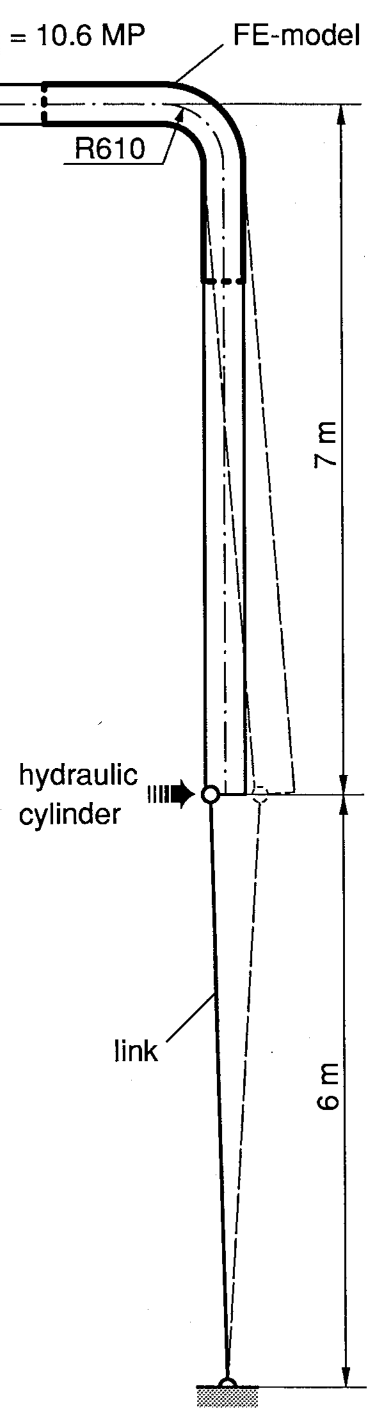

Figure 1 Test piping used for the RORV(B) full scale experiment.

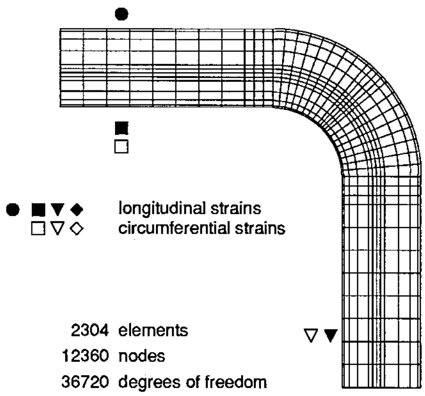

Figure 4 Strain gauge locations in the straight pipe ends and finite element mesh of the uncracked pipe bend.

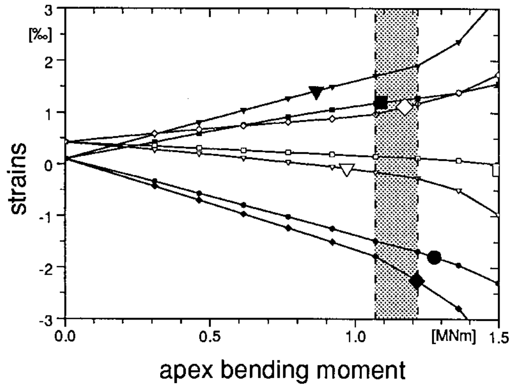

Figure 5 Calculated strains (small symbols) and measured data (large symbols) at strain gauge locations (Figure 4).

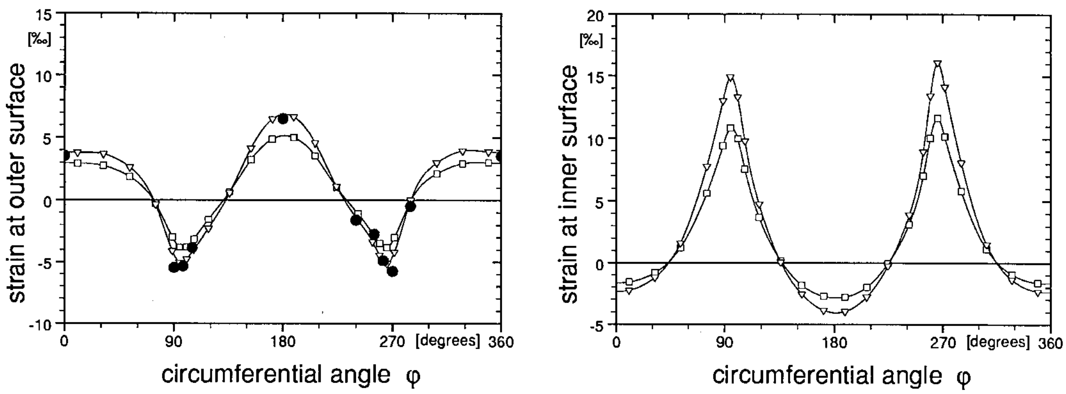

Figure 6 Calculated *circumferential strains* in the elbow apex ($\alpha = 45°$) due to the apex bending moments M = 1.07 MNm (squares) and M = 1.22 MNm (triangles), compared to maximum measured strains (filled circles).

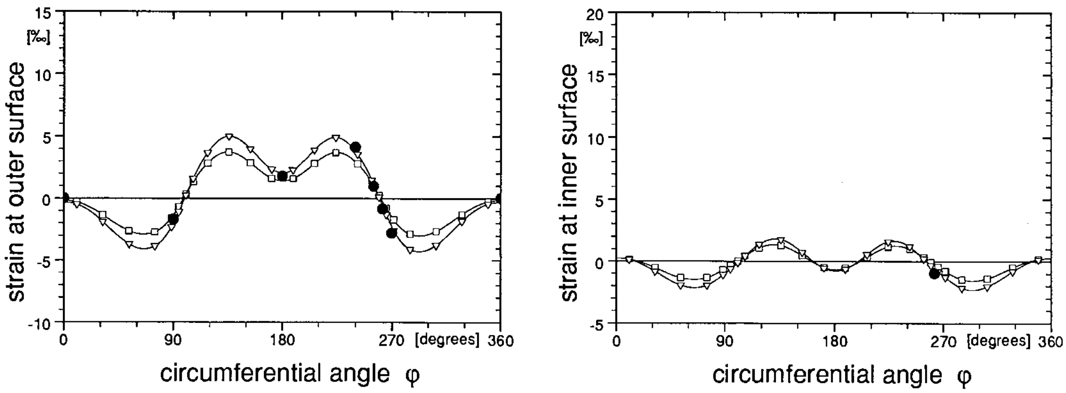

Figure 7 Calculated *longitudinal strains* in the elbow apex ($\alpha = 45°$) due to the apex bending moments M = 1.07 MNm (squares) and M = 1.22 MNm (triangles) compared to maximum measured strains (filled circles).

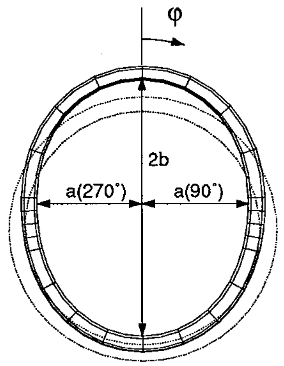

Figure 8 Cross-section at $\alpha = 45°$, undeformed and for an apex bending moment M = 1.22 MNm (deformation amplification factor = 3).

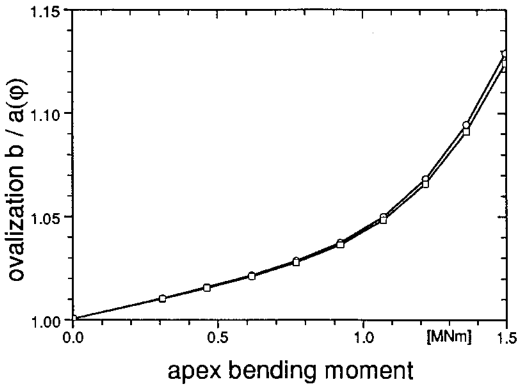

Figure 9 Cross-section ovalization $b/a(90°)$ (squares) and $b/a(270°)$ (circles) versus load.

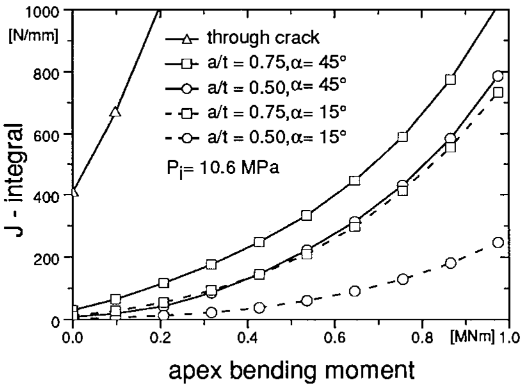

Figure 10 J at surface and at deepest point of the surface crack and J values for a through crack.

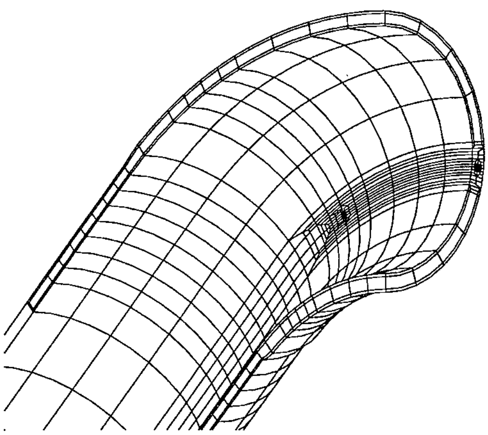

Figure 11 Finite element mesh used for crack analysis.

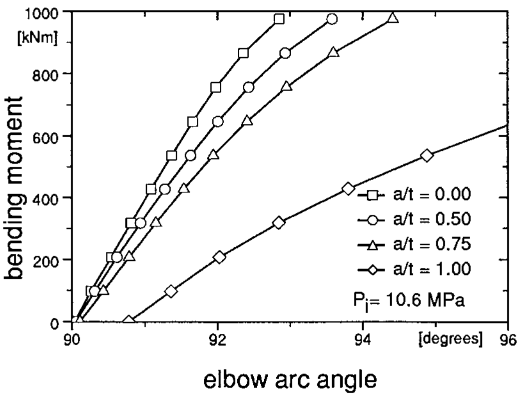

Figure 12 Elbow flexibilty for a crack length of $2\alpha_c = 60°$and different crack depths.

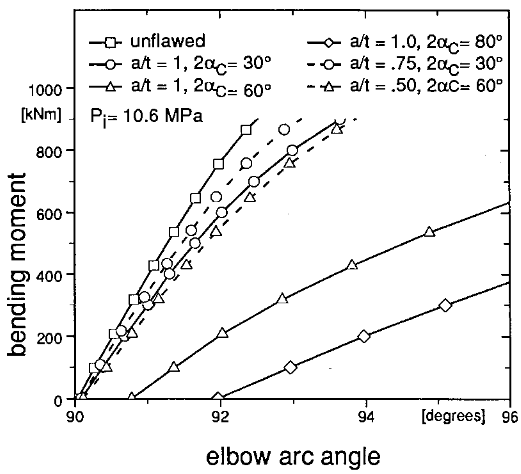

Figure 13 Elbow flexibility for different crack lengths and crack depths.